Lithium–Sulfur Battery State-of-Charge Observability Analysis and Estimation

Abbas Fotouhi, *Member, IEEE*, Daniel J. Auger, *Senior Member, IEEE*, Karsten Propp, and Stefano Longo, *Senior Member, IEEE*

***Abstract*—Lithium–Sulfur (Li–S) battery technology is considered for an application in an electric-vehicle energy storage system in this study. A new type of Li-S cell is tested by applying load current and measuring cell's terminal voltage in order to parameterize an equivalent circuit network model. Having the cell's model, the possibility of state-of-charge (SOC) estimation is assessed by performing an observability analysis. The results demonstrate that the Li–S cell model is not fully observable because of the particular shape of cell's open-circuit voltage curve. This feature distinguishes Li-S batteries from many other types of battery, e.g., Li-ion and NiMH. As a consequence, a Li-S cell's SOC cannot be estimated using existing methods in the literature and special considerations are needed. To solve this problem, a new framework is proposed consisting of online battery parameter identification in conjunction with an estimator that is trained to use the identified parameters to predict SOC. The identification part is based on the well-known prediction-error minimization algorithm; and the SOC estimator part is an adaptive neuro-fuzzy inference system in combination with coulomb counting. Using the proposed method, a Li-S cell's SOC is estimated with a mean error of 4% and maximum error of 7% in a realistic driving scenario.**

***Index Terms*—Adaptive neuro-fuzzy inference system (ANFIS), lithium–sulfur (Li-S) battery, model identification, observability analysis, state-of-charge (SOC) estimation.**

I. Introduction

DEVELOPMENT of energy storage systems can be considered as the heart of vehicle electrification process. Different new technologies for batteries, fuel cells, ultracapacitors, etc., are developing to be implemented in electric vehicles (EVs). One such new energy storage technology is the Lithium–Sulfur (Li-S) battery. Compared to incumbent Li-ion technologies, Li-S batteries have higher specific energy, improved safety, wider operational temperature range, and – when productionized – a lower unit cost due to the wide availability of sulfur, and consequently, Li-S is receiving serious research attention. The technology has not been commercialized yet because it suffers from limitations such as poor instantaneous power capabilities, high self-discharge, and short cycle life, particularly in the presence of high discharge currents [1], which are especially important for automotive applications [2]. Li-S technology has developed dramatically, though it has not yet been deployed in a full-scale EV to date mainly due to its insufficient power output and lifetime. There are, however, efforts to improve battery chemistry and construction to mitigate these problems. This work was undertaken as a part of an industrial project, aiming to develop and deploy experimental Li-S cells in an automotive application. Regardless of the state of development of the chemistry, it is important to be able to operate cells in practical applications, and this study is focused on Li-S cell parameter identification and state-of-charge (SOC) estimation.

There are different methods in the literature for battery SOC estimation [3]–[5]. Good reviews of these methods can be found in [6] and [7]. The most widespread conventional method, used as a benchmark for evaluation of other techniques, is "coulomb-counting." In this concept, an SOC is estimated by integrating the load current; this way, capacity used and remaining can be estimated. Assuming SOC_0 as the initial SOC at time t_0, the cell's SOC at time t is calculated as follows:

$$\mathrm{SOC} = \mathrm{SOC}_0 - \left(\int_{t_0}^{t} \frac{\gamma\, i(\tau)}{C_t} d\tau \right) \quad 0 < \mathrm{SOC} < 1 \qquad (1)$$

where $i(t)$ is the current (A) assumed positive for discharging and negative for charging. γ is the cell's coulombic efficiency (dimensionless) and C_t is the total capacity (As). In this representation, the SOC value is a number between 0 and 1 with 0 indicating a fully depleted state and 1 representing a fully charged state.

Although coulomb-counting is quite useful, it cannot always be used in practice because it can only start to estimate from a given initial SOC value. In many applications, batteries do not begin to discharge from fully charged state due to internal self-discharge or being not originally fully charged [8]. Generally, coulomb-counting suffers from accumulated errors caused by initial SOC value errors, and noise and measurement errors [9], [10]. Another problem is that the battery capacity (C_t) might change under various conditions (e.g., temperature variation), which can lead to errors when using coulomb-counting.

Another popular method for battery SOC estimation is the use of look-up tables or polynomials, which relate SOC to the battery's parameters. The most common parameter for this purpose is the battery's open-circuit-voltage (OCV). This method

Manuscript received May 6, 2017; accepted August 4, 2017. Date of publication September 27, 2017; date of current version March 5, 2018. Recommended for publication by Associate Editor Pavol Bauer. *(Corresponding Author: Abbas Fotouhi.)*

The authors are with the Advanced Vehicle Engineering Centre, Cranfield University, Cranfield MK43 0AL, U.K. (e-mail: a.fotouhi@cranfield.ac.uk; abfotouhi@gmail.com; d.j.auger@cranfield.ac.uk; k.propp@cranfield.ac.uk; s.longo@cranfield.ac.uk).

Color versions of one or more of the figures in this paper are available online at http://ieeexplore.ieee.org.

Digital Object Identifier 10.1109/TPEL.2017.2740223

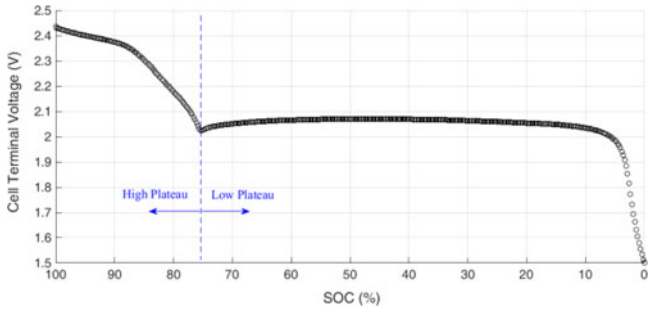

Fig. 1. Li-S cell terminal voltage during slow discharge at C/30.

also suffers from limitations. All possible conditions should be taken into consideration during the design process and the system might not be able to handle new and unknown conditions such as ageing effects. A large volume of test data is needed to cover all the possible variables such as SOC, temperature, ageing, current demand, and so on. Although, this method has been used very successfully for some battery types in previous studies, it is not easily applicable for a Li-S battery. The reason is the large flat region in OCV-SOC curve of this type of batteries as shown in Fig. 1.

Another group of existing SOC estimation algorithms are recursive adaptive filters such as particle filter and Kalman filter-based SOC estimators [11]–[15], which are particularly used for automotive application as well [16]–[19]. In this category, which is the most widely used technique of battery SOC estimation, the estimator works based on the error between the battery output (usually battery terminal voltage) and a battery model's prediction. The prediction error is usually large initially and it decreases gradually after a number of steps. So an accurate battery model is needed in this method that is able to predict battery terminal voltage well. The battery model contains the relationship between SOC and other parameters. There are many studies in the literature in which Li-ion battery models are used beside an SOC estimator [20]–[22]. However, similar studies have not been conducted for Li-S batteries yet. All of the developed Li-S battery models are electrochemical, which are too complex to be used in real-time applications. (The application of Kalman filters in Li-S cell SOC estimation has been considered in our project and results will be published in due course; however it is not in the scope of this article.)

In this study, the possibility of building an SOC estimator for a Li-S cell is investigated using a new approach. An observability analysis is performed for SOC estimation, which demonstrates the difference between Li-S and other battery types. The results demonstrate that the common SOC estimation methods in the literature may not be applicable for Li-S cell because of its unique features. To solve this problem, a combination of system identification technique, artificial intelligence, and coulomb-counting is utilized in this study. Pure coulomb-counting is used as a bench mark to evaluate the estimation results. Because of the application of this study in EVs, the goal is to have a simple and fast method that is applicable in real-time. So the minimum number of parameters is considered for model identification. The selected parameters are internal resistance and OCV.

TABLE I
SPECIFICATIONS OF LI-S CELL

Parameter	Description
Type	Rechargeable lithium-sulfur pouch cell Remarks: Li Metal Anode
Nominal dimension	145 mm × 78 mm × 5.6 mm
Applications	Recommended discharge current: 680 mA
Nominal voltage	2.05 V
Capacity	Typical: 3400 mAh when discharged at 680 mA to 1.5 V at 30 °C
Charging condition	340 mA to 2.45 V at 30 °C
Recommended charging condition in applications	340 mA constant current (C/10) Charge termination control recommended: charge stop at 2.45 V or 11 h max charge time
Clamped charging voltage	2.45 V ± 0.05 V
Service life	>95 cycles at 100% depth of discharge >150 cycles at 80% depth of discharge
Weight	Approx. 50.7 g
Ambient temperature range	Charge/ Discharge: 5 °C to 80 °C Storage (1 year): –27 °C to 30 °C

The identification results are then utilized for cell's SOC estimation. Prediction-error minimization (PEM) algorithm and adaptive neuro-fuzzy inference system (ANFIS) in combination with coulomb counting are used for model identification and SOC estimation, respectively. The PEM is a fast identification algorithm in which the prediction error (as a function of the model's parameters) is minimized using an iterative procedure [23]. ANFIS is a powerful tool for modeling, prediction, and control by integrating synergy of the artificial neural network and the fuzzy logic. A fuzzy set (which works based on fuzzy logic) is an efficient tool for modeling of a phenomenon related to human knowledge by using linguistic labels that are embedded in a number of membership functions. A fuzzy inference system (FIS) is a collection of fuzzy if-then rules, which contains human expertise and knowledge. Because a FIS does not have learning and adaptation capabilities, neuro-fuzzy techniques have been developed in order to add this functionality to FIS too. A hybrid learning approach is used in ANFIS structure that combines the gradient-descent and the least squares methods for the parameter tuning. ANFIS has been used in a wide range of applications and particularly, it has been used for battery SOC estimation in previous studies [24], [25]. In this study, ANFIS has been used in combination with coulomb counting to estimate SOC of Li-S battery chemistry for the first time.

II. EXPERIMENTAL TESTS ON LI-S CELL

The Li-S cells considered in this study were supplied by OXIS Energy Ltd., Abingdon, U.K., [26] with the specifications in Table I. It should be noted that the tested cell in this study was a prototype cell with lower energy density (around 140 Wh/kg) than the final product that is expected to have an

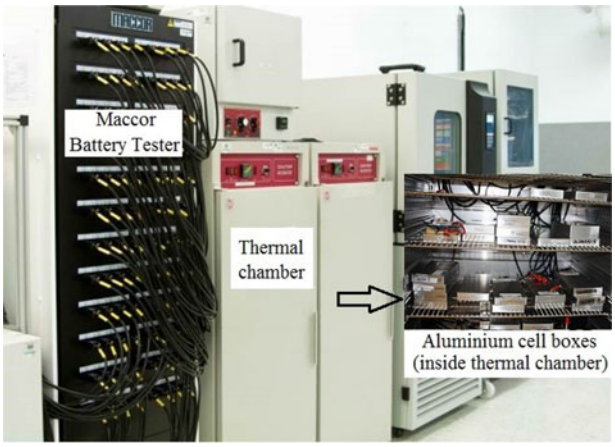

Fig. 2. Cell test equipment.

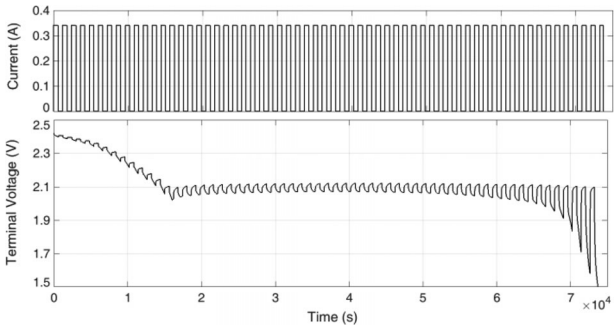

Fig. 3. Load current (input) and Li-S cell's terminal voltage (output) during an experiment.

energy density more than 400 Wh/kg [26]. A Maccor Series-4000 battery tester was used for all experiments. The battery tester is a voltage/current device which can apply a current as an "input" and measures the voltage as an "output" (or indeed vice versa). The current and voltage limits are ±5 A and ±5 V for each channel. The cell under test is contained inside an aluminum test box, which is connected to the equipment. The test box is placed inside a Binder thermal chamber to set the desired temperature during each test. The cell test equipment is depicted in Fig. 2.

Experiments are conducted by applying consecutive discharge current pulses to the battery and measuring terminal voltage as the output. Each test starts from fully charged state (2.4 V) and continues until the terminal voltage drops below the cutoff voltage (1.5 V). Accordingly, cell parametrization is possible at different SOC levels. Between the consecutive pulses, a "relaxation time" is allowed, during which the current is zero. Data are collected in the time domain with a sampling rate of 1 Hz. The measurements available include time, temperature, current, and terminal voltage. In Fig. 3, cell measurements including load current (input) and terminal voltage (output), which are recorded at 25 °C, are shown for an experiment.

III. Li-S Cell Parameter Identification

In this section, an equivalent-circuit-network (ECN) model is parameterized using experimental data from Li-S cells. The goal

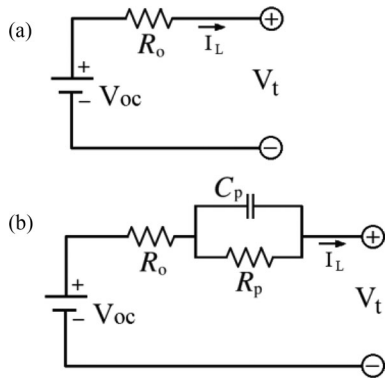

Fig. 4. Equivalent circuit battery models. (a) Internal resistance model. (b) Thevenin model (1RC model).

of this study is not building a "descriptive model," which is able to accurately determine battery terminal voltage (output) subject to a load current (input), but it aims at making a simple model for SOC estimation. So, an ECN modeling approach [27]–[29] is selected. A review on different battery modeling approaches can be found in [27]. An ECN model is constructed by putting resistors, capacitors, and voltage sources in a circuit to model the battery's performance. Here the simplest form of an equivalent circuit battery model is used, which is the internal resistance model ($R_{\rm int}$ model) [30]. As depicted in Fig. 4(a), the model's unknown parameters are cell's ohmic resistance (R_O) and cell's OCV ($V_{\rm OC}$). Load current (i_L) and cell's terminal voltage (V_t) are model's measured input and output, respectively.

The PEM algorithm [23] is utilized as the identification algorithm. For a sufficiently economical model structure, PEM is fast enough to be used in real-time applications such as a battery management system (BMS). In the identification procedure, the model parameter vector (θ) is determined so that the prediction error (ε) is minimized, which is defined as follows:

$$\varepsilon(t_k,\theta) = y(t_k) - \hat{y}(t_k|\,t_{k-1};\theta) \tag{2}$$

where $y(t_k)$ is the real output at time k and $\hat{y}(t_k|t_{k-1}\,;\theta)$ is predicted value of the output at time k using the parameters θ. The prediction error depends on the parameter vector, so an iterative minimization procedure has to be applied. Consequently a scalar fitness function is minimized as follows:

$$E_N(\theta) = \det\left(\frac{1}{N}\sum_{k=1}^{N}\varepsilon(t_k,\theta)\,\varepsilon^T(t_k,\theta)\right). \tag{3}$$

In this study, the parameters vector contains cell's internal resistance and OCV. The parameters are optimized so that the least difference between measured terminal voltage (V_t) and model's output is achieved

$$\theta = [R_O\ ,\ V_{\rm OC}] \tag{4}$$

$$\varepsilon(t_k,\theta) = V_t(t_k) - \hat{V}_t(t_k|\,t_{k-1};\theta). \tag{5}$$

The battery is a nonlinear system whose parameters change slowly according to states and inputs, so the model's parameters need to be updated at regular "time intervals" or "SOC intervals."

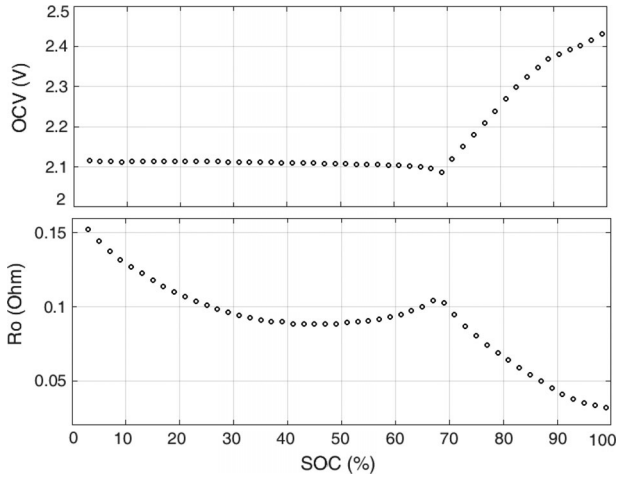

Fig. 5. Li-S cell's internal resistance and OCV at different SOC.

A short time history of battery input–output measurements is used for parameter identification. Because of the variations of power demand in an EV, a straightforward fixed time interval is not suitable here. Instead, an application-specific combination of an SOC interval and a time interval was designed and used in order to prevent numerical problems at high discharge rates. In this approach, the identification is repeated based on SOC intervals (i.e., 1%) while a minimum time length is guaranteed for the identification interval (i.e., 120 s). In this way, when the length of the SOC window is less than the minimum time window value, the identification interval is expanded to the minimum time.

Li-S cell's internal resistance and OCV are obtained for the experiment described in previous section (see Fig. 3). Referring to Fig. 1, the Li-S SOC range can be divided into two parts, usually referred to as the "high plateau" (HP) and "low plateau" (LP). There is a breakpoint at around 75% SOC that determines the boundary between the two plateaus. This transition, which is caused by a sudden change in electrochemical reactions inside the Li-S cell, might shift slightly to the right or left under different discharge conditions. The identification results are also in accordance with the expected pattern of OCV as illustrated in Fig. 5. The final part of the OCV plot in Fig. 5 does not drop as far as it could because the test is not continued to completely depleted state since the experimental equipment stops test procedures at a cutoff voltage of 1.5 V to protect the cell from damage.

The pattern of the Li-S cell's internal resistance variation versus SOC is depicted in Fig. 5. The internal resistance has its least value at very high SOC and it increases as SOC decreases within the HP until the breakpoint. In the LP, the curve is almost parabolic and a minimum resistance point exists as illustrated in Fig. 5. Independent of the application in SOC estimation, this identification results are valuable for other applications such as optimum charge/discharge of Li-S batteries and BMS design.

IV. SOC Observability Analysis

In this section, an observability analysis is performed in order to demonstrate the difference between Li-S cell and other battery types. NiMH battery data [34] is used as another type of battery for comparison. The goal is to investigate the possibility of Li-S cell SOC estimation using the existing classical methods in the literature. For this purpose, an equivalent circuit battery model, called "Thevenin model" [33] or one RC network model (1RC model), is used as illustrated in Fig. 4(b). In this structure, V_t is battery's terminal voltage, $V_{\rm OC}$ is OCV, R_O is internal resistance, R_P and C_P are equivalent polarization resistance and capacitance, respectively. The dynamic equations of such a model are

$$\begin{cases} V_t = V_{\rm OC} - R_O\, I_L - V_P \\ \frac{dV_P}{\rm dt} = -\frac{1}{R_P\, C_P} V_P + \frac{1}{C_P} I_L. \end{cases} \tag{6}$$

Using the above differential equations, an observability analysis would be possible by considering a state-space representation of the model

$$\begin{aligned} \mathbf{y}\,(t) &= \mathbf{C}\mathbf{x}\,(t) + \mathbf{D}\mathbf{u}\,(t) \\ \dot{\mathbf{x}}\,(t) &= \mathbf{A}\mathbf{x}\,(t) + \mathbf{B}\mathbf{u}\,(t) \end{aligned} \tag{7}$$

where $\mathbf{y}(t) \in R^N$ is a time-dependent vector of measurable outputs, $\mathbf{u}(t) \in R^M$ is a time-dependent vector of inputs, $\mathbf{x}(t) \in R^K$ is a time-dependent state vector, and the matrices $\mathbf{A} \in R^{K\times K}$, $\mathbf{B} \in R^{K\times M}$, $\mathbf{C} \in R^{N\times K}$, and $\mathbf{D} \in R^{N\times M}$ define the system's behavior.

For model linearization, a method, which is proposed in [22], is used here. Let X denote the state of charge, V_P and X are model's states, current is the input and terminal voltage is the output. For V_P, it is easy to write it in the standard state-space format; however, there is more to do for SOC. Using coulomb-counting, an SOC is calculated by integrating the load current. There is still one term in the output equation that is not match with the standard form of state-space. OCV can be obtained as a nonlinear function of X based on the identification results. Such a nonlinear function can be divided into small linear parts using the gain scheduling method developed in [31]. Considering $\Delta_{\rm SOC}$ as the SOC interval length, battery OCV can be written for the ith SOC interval as follows:

$$\begin{aligned} V_{\rm OC} &= a_i\,.\,X_i\, +\, b_i \\ &\qquad \text{where } (i-1).\,\Delta_{\rm SOC} \le X_i \le i.\,\Delta_{\rm SOC}. \end{aligned} \tag{8}$$

The coefficients *a* and *b* are obtained from OCV-SOC curve and are constant at each small segment as illustrated in Fig. 6. So OCV can be replaced by its linearized approximation in the output equation as follows:

$$V_t = a_i.\,X + b_i - R_O\, I_L - V_P. \tag{9}$$

Consequently, the state-space representation of the battery model is

$$\begin{cases} \begin{bmatrix} \frac{dV_P}{\rm dt} \\ \frac{dX}{\rm dt} \end{bmatrix} = \begin{bmatrix} -\frac{1}{R_P\, C_P} & 0 \\ 0 & 0 \end{bmatrix} \begin{bmatrix} V_P \\ X \end{bmatrix} + \begin{bmatrix} \frac{1}{C_P} \\ \frac{\eta}{C_t} \end{bmatrix} I_L \\ V_t - b_i = \begin{bmatrix} -1 & a_i \end{bmatrix} \begin{bmatrix} V_P \\ X \end{bmatrix} - R_O\, I_L. \end{cases} \tag{10}$$

To be observable, it must be possible to infer a system's internal state from its measurable outputs alone. For a system in

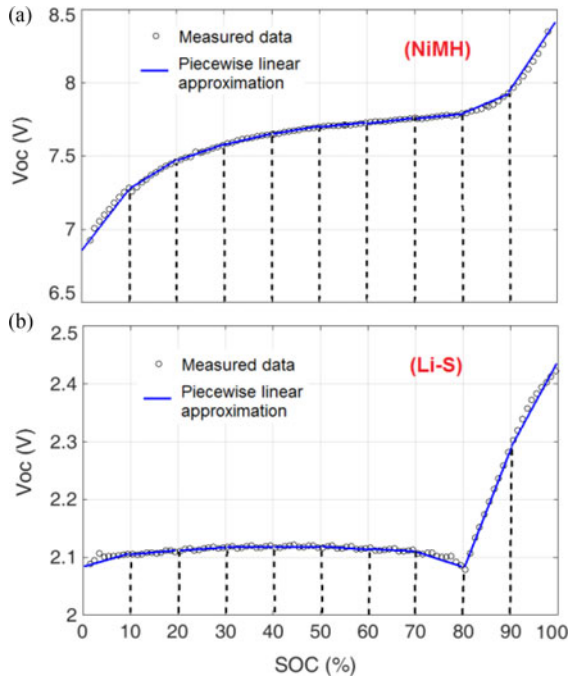

Fig. 6. Piecewise linear approximation of OCV-SOC curves. (a) NiMH. (b) Li-S.

state-space representation to be observable, it is necessary and sufficient that the "observability gramian" has full column rank

$$\mathbf{W}_{\mathrm{o}} := \begin{bmatrix} \mathbf{C} \\ \mathbf{CA} \\ \mathbf{CA}^2 \\ \vdots \\ \mathbf{CA}^{K-1} \end{bmatrix} \tag{11}$$

where K is the dimension of the state vector. If $\mathbf{W}_{\mathrm{o}}$ has a poor condition number (i.e., is close to not having full column rank), then observability will be poor [32]. The battery model's observability matrix is obtained as follows:

$$\mathbf{W}_{\mathrm{o}} := \begin{bmatrix} C \\ CA \end{bmatrix} = \begin{bmatrix} -1 & a_i \\ \frac{1}{R_P C_P} & 0 \end{bmatrix}. \tag{12}$$

Since R_P and C_P are positive nonzero numbers in the battery models, the only case in which the observability matrix is not full rank is when a_i be zero. This will never happen for a NiMH battery model because of its OCV-SOC characteristics as shown in Fig. 6. More details of the test data of NiMH battery can be found in [34]. For a Li-ion battery model, an SOC is also observable as discussed in [22]. However, our results demonstrate that the system is not fully observable for the case of Li-S because of the particular features of Li-S battery OCV curve. Indeed, the coefficient a_i can be zero for a Li-S battery. The whole range of SOC of a Li-S battery can be divided into two parts called HP and LP. Li-S cell SOC cannot be estimated using OCV curve in LP because of its flat shape as depicted in Fig. 6. This is a unique feature of Li-S battery, which distinguishes it from other battery types. Preliminary results of this discussion has been presented in [35], which is focused on the comparison between NiMH and Li-S batteries from the control engineering point of view.

The above mentioned problem may be solved by using other parameters in addition to OCV. In the following, a more general mathematical formulation is presented to demonstrate the idea of using other parameters for Li-S cell SOC estimation. Consider the data required for a typical parameter identification study. Let Θ_i be the set of parameters that have been identified; this could be via PEM or any other method. Our parameter vector is

$$\mathbf{\Theta} = \begin{bmatrix} \Theta_1 & \Theta_2 & \cdots & \Theta_N \end{bmatrix}^{\mathrm{T}}. \tag{13}$$

The parameter identification process is the measuring device! and the dynamic state, which we wish to infer, is SOC. It is assumed that the parameters are functions of SOC by ignoring other parameters such as temperature for the time being. Each parameter is a function of

$$\Theta_i = h_i\left(X\right)$$

or expressed in a vector sense

$$\mathbf{\Theta} = \mathbf{h}\left(X\right). \tag{14}$$

The dynamics of interest are solely the SOC dynamics, Here

$$\dot{X}\left(t\right) = f\left(X, I_{\mathrm{L}}\left(t\right)\right) = -\frac{1}{Q_{\mathrm{cap}}} I_{\mathrm{L}}\left(t\right) \tag{15}$$

where I_{L} is the load current (amperes) and Q_{cap} is the capacity of the cell or battery (coulombs).

To determine the observability of the system, we must define an "operating point," say, $(\bar{X}, \bar{I})$, with a corresponding parameter set $\bar{\mathbf{\Theta}}$. We can then define perturbation variables

$$\begin{aligned} \mathbf{\Theta}\left(t\right) &= \bar{\mathbf{\Theta}} + \hat{\theta}\left(t\right) \\ X\left(t\right) &= \bar{X} + \hat{\chi}\left(t\right) \\ I\left(t\right) &= \bar{I} + \hat{i}\left(t\right). \end{aligned} \tag{16}$$

We can then write down an expression for a linearized model

$$\hat{\theta}\left(\mathrm{t}\right) \approx \underbrace{\begin{bmatrix} \partial h_1/\partial \mathrm{X} \\ \partial h_2/\partial \mathrm{X} \\ \vdots \\ \partial h_N/\partial \mathrm{X} \end{bmatrix}}_{\mathrm{c}} \hat{\chi}\left(\mathrm{t}\right) \tag{17}$$

$$\hat{\chi} \approx \underbrace{\left(\frac{\partial f}{\partial X}\right)}_{A} \hat{\chi}\left(t\right) + \underbrace{\left(\frac{\partial f}{\partial I}\right)}_{B} \hat{i}\left(t\right) \tag{18}$$

noting that

$$\frac{\partial f}{\partial X} = 0 \Rightarrow A = 0. \tag{19}$$

We can then form the observability grammian for our system. As we have one dynamic state

$$\mathbf{w}_{\mathrm{o}} = \mathbf{c} = \begin{bmatrix} \partial \mathrm{h}_1/\partial \mathrm{X} \\ \partial \mathrm{h}_2/\partial \mathrm{X} \\ \vdots \\ \partial \mathrm{h}_{\mathrm{N}}/\partial \mathrm{X} \end{bmatrix}. \tag{20}$$

The system will be observable if and only if this has full column rank. Fortunately, "full rank" in this case means a rank of one. In general, the SOC will be observable providing that

$$\frac{\partial \mathrm{h_i}}{\partial \Theta_i} \neq 0 \tag{21}$$

for at least one parameter Θ_i.

If we consider a battery model where the only parameter that is estimated is the open-circuit voltage (V_{oc}), then

$$W_{\mathrm{o}} = [\partial \mathrm{h}_{V_{\mathrm{oc}}} / \partial \mathrm{X}] \tag{22}$$

where

$$V_{\mathrm{oc}} = \mathrm{h}_{V_{\mathrm{oc}}}(X). \tag{23}$$

This will have full rank unless the open-circuit voltage "plateaus" and remains constant; unfortunately, with Li-S cell, this is exactly what happens. During this part of the charge/discharge cycle, the SOC is not observable from a measurement of open-circuit voltage alone.

If instead we consider a scenario where a second parameter is estimated, internal resistance (R_{o}) for example, then we get

$$\mathbf{w}_{\mathrm{o}} = \begin{bmatrix} \partial \mathrm{h}_{V_{\mathrm{oc}}} / \partial \mathrm{X} \\ \partial \mathrm{h}_{R_{\mathrm{o}}} / \partial \mathrm{X} \end{bmatrix} \tag{24}$$

where

$$R_{\mathrm{o}} = \mathrm{h}_{R_{\mathrm{o}}}(X). \tag{25}$$

This will have full rank unless

$$\frac{\partial \mathrm{h}_{V_{\mathrm{oc}}}}{\partial \mathrm{X}} = \frac{\partial \mathrm{h}_{R_{\mathrm{o}}}}{\partial \mathrm{X}} = 0. \tag{26}$$

If this occurs at all, this is a transient situation so there is no prolonged loss of observability. Accordingly, it is clear that having open-circuit voltage alone is insufficient for Li-S cell state estimation, but adding other parameters like internal resistance can make the system observable.

V. Li-S Cell SOC Estimation Using ANFIS

As discussed in the previous section, a Li-S cell's SOC estimation is more challenging than many other types of battery because of observability limitations. For this reason, a framework is developed in this study based on fast online battery parameter identification. The idea is to identify battery parameters in real-time and use them as an indicator of SOC. So we need to find the relationship between the identification results and SOC by using a mapping tool, which is ANFIS. (It should be noted that other mapping tools may also be applicable as well as ANFIS.)

Before explaining the ANFIS structure, the proposed framework is discussed as follows. It is demonstrated in the literature that battery's performance is a function of different factors such as SOC, state of health (SOH) [36], and temperature. So generally cell's parameters are functions of those variables as follows:

$$P_i = f_i(\mathrm{SOC}, \mathrm{SOH}, T, ...) \quad i = 1..n. \tag{27}$$

The number of parameters and variables that are used in a battery model depends on the required precision. In some cases, high-fidelity models are needed whereas a fast low-fidelity model is desired in other cases. In this study, a simple and fast model is needed for real-time SOC estimation. The idea of SOC estimation is to find an inverse function, which is able to predict SOC by using the identified parameters. Being aware of the influence of SOH and temperature on our results, we assume fixed values for these variables and plan to extend our algorithms in our future works. So the following equations are used for the sake of simplicity

$$P_i = f_i(\mathrm{SOC}) \quad i = 1..n. \tag{28}$$

The battery parameters are obtained by using the system identification algorithm and, then a nonlinear function like g, in following equation, (i.e., ANFIS) is utilized for SOC estimation:

$$\mathrm{SOC} = g(P_1, P_2, .., P_n). \tag{29}$$

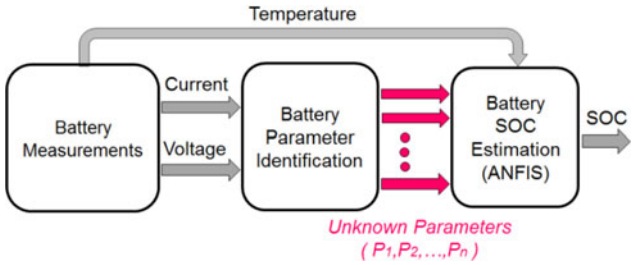

Fig. 7. Battery measurement, identification, and SOC estimation.

Schematic of the whole procedure is depicted in Fig. 7, which includes real-time measurement, identification, and SOC estimation. The advantages of the proposed framework can be summarized as follows.

1) It is a flexible framework that can be applied to various battery types (It is demonstrated how it can even handle the flat OCV curve of a Li-S cell).
2) Unlike coulomb-counting, it can start from any initial SOC value and no initial condition data are needed to run the estimator.
3) Unlike coulomb-counting, the whole battery capacity is not needed for SOC calculation.
4) Unlike recursive adaptive filters, no time is needed for convergence of the algorithm at the beginning.
5) The proposed method is simple and fast enough to be used in real-time applications. In addition, ANFIS models are adaptive and can be retuned very fast.

For Li-S SOC estimation, the experiments are performed on three similar cells. The first is used for ANFIS training and the other two are used for evaluation. During the training process, ANFIS components including weight numbers and membership functions (MFs) parameters are tuned. The ANFIS parameters are optimized so that the least error exists between the real SOC values (obtained by coulomb-counting) and ANFIS estimation.

Since the simplest ANFIS structure is desired, different structures are investigated by changing the number of inputs. First, just one input is considered: OCV. The estimation results using just OCV are demonstrated in Fig. 8 where the actual SOC and ANFIS estimations are compared for (a) training data, (b) test

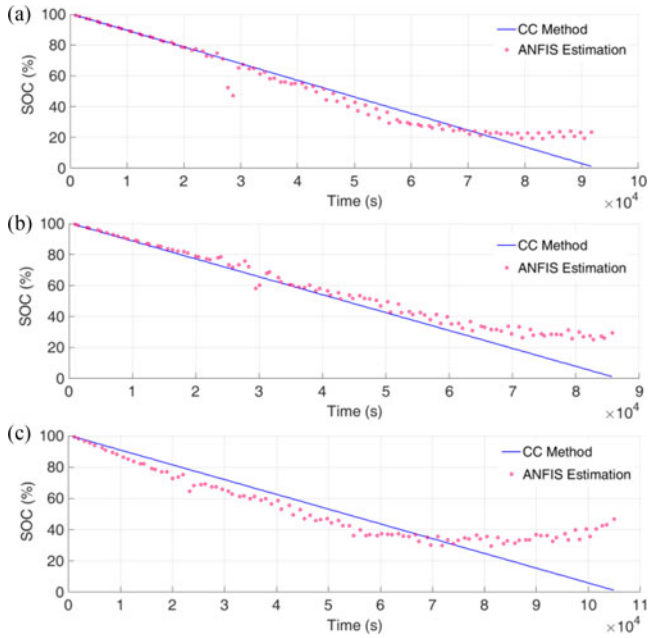

Fig. 8. Actual SOC and ANFIS estimations using $V_{\rm OC}$. (a) Training data. (b) Test data 1. (c) Test data 2.

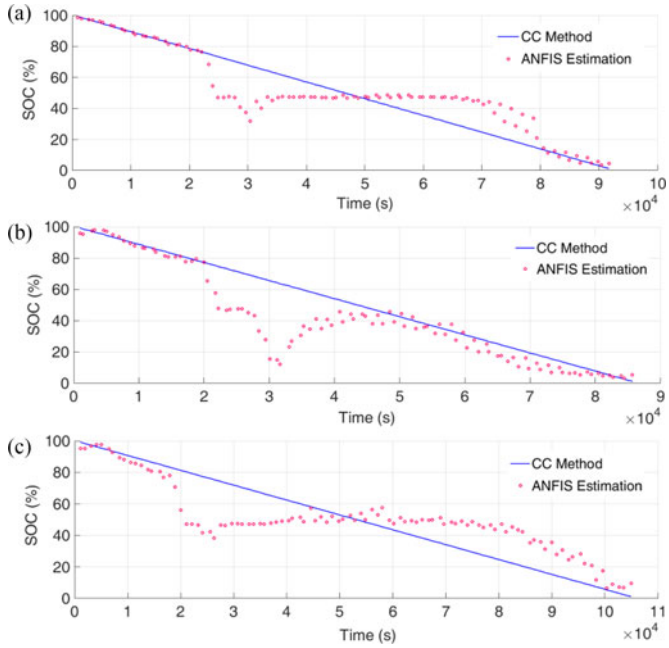

Fig. 9. Actual SOC and ANFIS estimations using R_O. (a) Training data. (b) Test data 1. (c) Test data 2.

data 1, and (c) test data 2. It should be noted that the three test data are obtained from three Li-S cells that makes the situation much difficult. The estimation accuracy is fine at HP; however, it is not satisfactory at LP because of the flat shape of OCV in this area.

In the second structure, R_O is used as the only input for ANFIS. Fig. 9 depicts the results in this case, which are not considered to be any better that the first case. This means that R_O also is not sufficient for SOC estimation and we need to

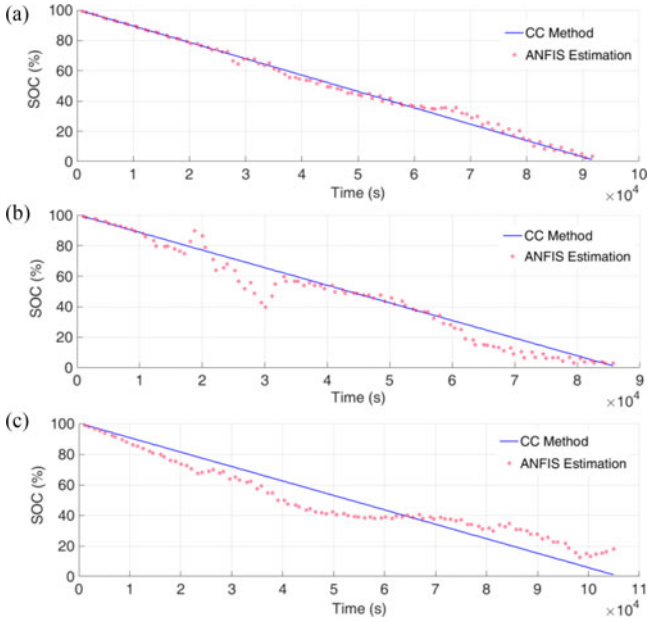

Fig. 10. Actual SOC and ANFIS estimations using $V_{\rm OC}$ and R_O. (a) Training data. (b) Test data 1. (c) Test data 2.

increase the complexity. The obvious choice at this stage is to use both R_O and $V_{\rm OC}$ at the same time. The results are much better in this case as demonstrated in Fig. 10. Especially for the training data [see Fig. 10(a)], the ANFIS structure is now able to learn and build the relation between the parameters and SOC. However, the test results are still not considered to represent satisfactory performance. The reason can be explained using the identification results shown in Fig. 5; in the HP, OCV is sufficient for SOC estimation, whereas in the LP, OCV does not provide useful information and the resistance curve alone appeared to be insufficient for SOC estimation. There are a number of possibilities here: essentially, more information is needed. This information can be provided by trying more parameters like R_P and C_P in Thevenin model for example [see Fig. 4(b)]. On the other hand, more complexity means less speed or more computational effort in real-time applications. To keep the same complexity while having more information for SOC estimation, a novel solution is proposed in this study; the derivative of resistance (with respect to SOC) is used as another input because it contains additional information that improves the estimation accuracy. So an SOC is determined by using the following three inputs

$$\mathrm{SOC} = g\left(R_O, \frac{dR_O}{d\mathrm{SoC}}, V_{\rm OC}\right). \tag{30}$$

The final structure of the inputs and output of ANFIS is illustrated in Fig. 11. As mentioned before, the inputs of ANFIS should be provided by the identification block (see Fig. 7). In this case, the inputs, $V_{\rm OC}$, R_O, and $dR_O/d\mathrm{SOC}$, must be first identified and, then SOC is estimated as the output of ANFIS. A generalized bell-shaped MF is selected for the inputs. A hybrid learning approach is used, combining the gradient-descent method with the least squares estimate to tune ANFIS parame-

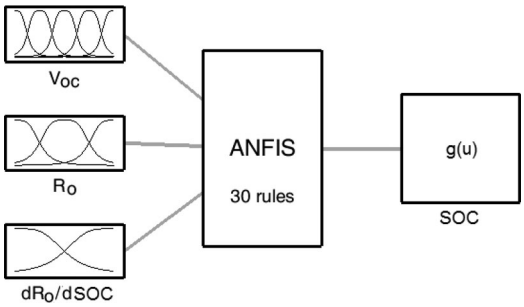

Fig. 11. ANFIS structure using 3 inputs and 30 rules.

TABLE II
ANFIS SPECIFICATIONS

Parameter	Description
Inputs	R_O, $dR_O/d\mathrm{SOC}$, V_{OC}
Output	SOC
Input MF type	generalized bell-shaped
Output MF type	Linear
Number of MFs	3, 2, 5
Number of rules	30
Training epoch number	500

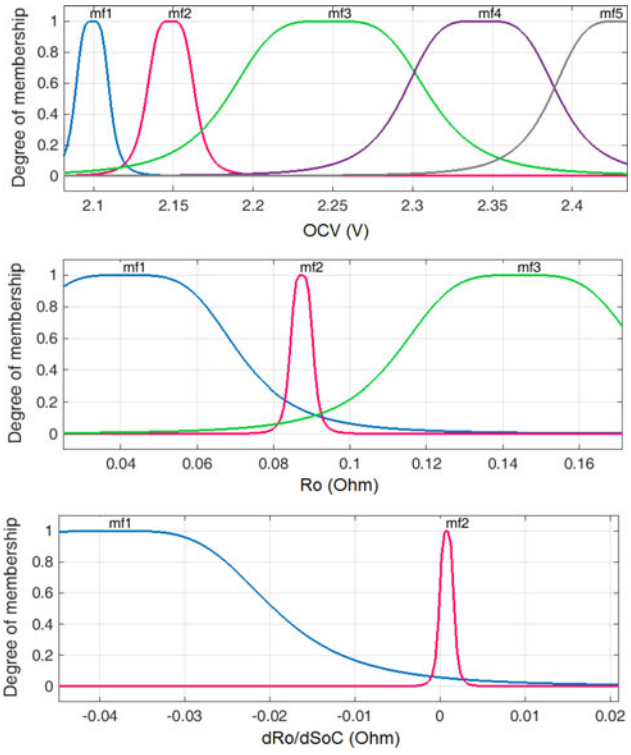

Fig. 12. ANFIS inputs MFs after training.

ters. Other specifications of the designed ANFIS are provided in Table II. As stated in Table II, the number of MFs used for R_O, $dR_O/d\mathrm{SOC}$, and V_{OC} inputs are 3, 2, and 5, respectively. MFs of the three inputs after training are illustrated in Fig. 12. Using more MFs for each input is possible; however, our results demonstrate that in this scenario, it would just increases complexity of the system without further improving the accuracy.

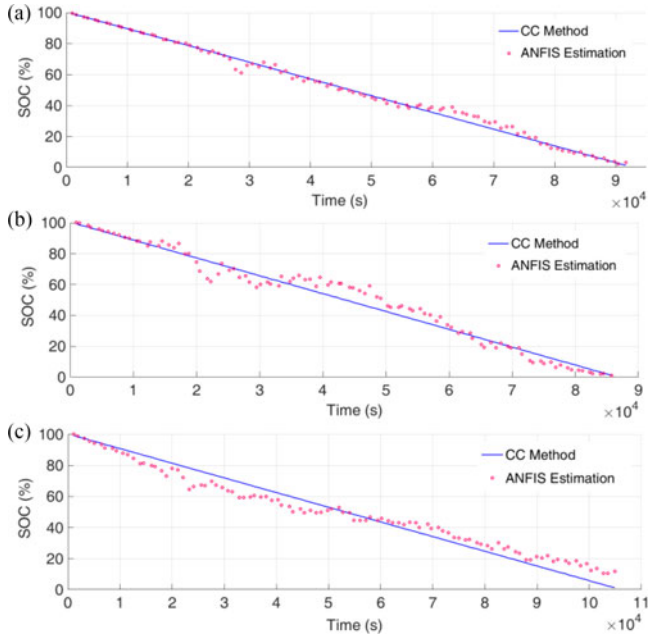

Fig. 13. Actual SOC and ANFIS estimations using V_{OC}, R_O, and $dR_O/d\mathrm{SOC}$. (a) Training data. (b) Test data 1. (c) Test data 2.

TABLE III
LI-S CELL SOC ESTIMATION ERROR USING ANFIS

Inputs	Number of Rules	Estimation Error (%) in Training Data	Estimation Error (%) in Test Data 1	Estimation Error (%) in Test Data 2
V_{OC}	9	Mean: 4.61 Max.: 22.21	Mean: 6.38 Max.: 28.28	Mean: 9.91 Max.: 45.25
R_O	9	Mean: 8.88 Max.: 35.55	Mean: 9.54 Max.: 51.39	Mean:12.82 Max.: 36.98
R_O, V_{OC}	35	Mean: 1.74 Max.: 8.08	Mean: 4.84 Max.: 25.61	Mean: 7.81 Max.: 16.87
R_O, V_{OC} $dR_O/d\mathrm{SOC}$	30	Mean: 1.55 Max.: 8.23	Mean: 3.93 Max.: 13.76	Mean: 5.11 Max.: 13.77

The results demonstrate that using these three inputs, a Li-S cell's SOC can be estimated with a good accuracy. For the training data, the average (mean) and maximum estimation errors are 1.55% and 8.23%, respectively. The actual and estimated values of SOC are compared in Fig. 13 for (a) training data, (b) test data 1, and (c) test data 2. For the two test data sets, error values are a bit more than the training data set, which usually happens in training such systems. Roughly, the proposed estimation method can predict SOC value with average and maximum errors of 5% and 14%, respectively. Table III contains all the estimation error values for different ANFIS structures.

Generally, it is very difficult to predict the exact location of the break point between HP and LP since it depends on many factors. In addition, the total capacity values in the experiments are different. The reason is the difference between the three cells which are used here. Li-S cell's capacity could change a lot under different conditions. Even for one cell, the break point's location and total capacity can change due to variation in temperature, discharge rate, etc., which make Li-S battery SOC estimation

a challenging task. The result that is presented in Fig. 13 and Table III is a first try for Li-S cell's SOC estimation and there is no similar work in the literature. In future works, the estimation capability will be extended to cover different temperature and ageing ranges.

VI. Case Study: Simulation and Test of Li-S Cell Based on Urban Dynamometer Driving Schedule (UDDS)

In a case study, performance of the proposed framework for Li-S cell parameter identification and SOC estimation is evaluated in a more realistic scenario for EV application. For this purpose, a new series of experimental tests were performed based on EV power demand on UDDS also known as U.S. FTP-72 (Federal Test Procedure) [37]. As the input of these tests, a typical EV (i.e., Nissan Leaf) was simulated on UDDS drive cycle. More details of EV modeling and simulation can be found in [34] and [38]. The power demand signal was, then, scaled-down to be applied to a single cell. Since the Li-S cells used in this study are prototypes; they cannot deliver a high power expected from an existing Li-ion or NiMH cell in the market. This does not affect our results and conclusions because the final cells will have same characteristics curves in shape. Average power of a single Li-S cell, which is used in this study, is about 5 W. Assuming a maximum power demand of 60 kW in a typical EV to move based on UDDS drive cycle, 12 000 of these prototype Li-S cells are needed. Based on this calculation, the power demand from a single cell is obtained by dividing the EV power by the number of cells. The Li-S cell was tested using scaled-down current profiles obtained from the EV simulation. Like the pulse discharge test explained in Section II, current and terminal voltage were recorded at sampling rate of 1 Hz.

Fig. 14 demonstrates a Li-S cell discharge test based on UDDS drive cycle. UDDS speed profile is illustrated at top, which is used to calculate the EV battery pack power demand. A scaled-down current profile is depicted in Fig. 14(b) in which the maximum current is around 1.2 A. Keeping same ratios, all current values can be scaled up and down to investigate different currents levels as well. In our tests, the maximum current was not more than 2.4 A. Fig. 14(c) shows terminal voltage of the Li-S cell during one UDDS cycle in response to the current demand. In Fig. 14(d) and (e), current profile and cell's terminal voltage are illustrated during the whole test. Each test is performed by repeating the UDDS cycle from 100% SOC to depleted state. Test time, which depends on the current profile, was more than 22 h in this case. A number of tests were conducted at different temperature and current levels. Fig. 15 demonstrates Li-S cell parametrization at 30 °C during three complete UDDS tests. These tests are performed under same conditions just the current level is higher in tests 2 and 3 as presented in Table IV. Cell parameters, V_{OC} and R_O, are identified over the whole tests to be used for SOC estimation by ANFIS. An error in the identification part will lead to an error in SOC estimation as well. The total SOC estimation error can be written as follows:

$$\text{SOC estimation error} = \text{SOC estimation error due to identification uncertainty} + \text{estimator (ANFIS) error} \tag{31}$$

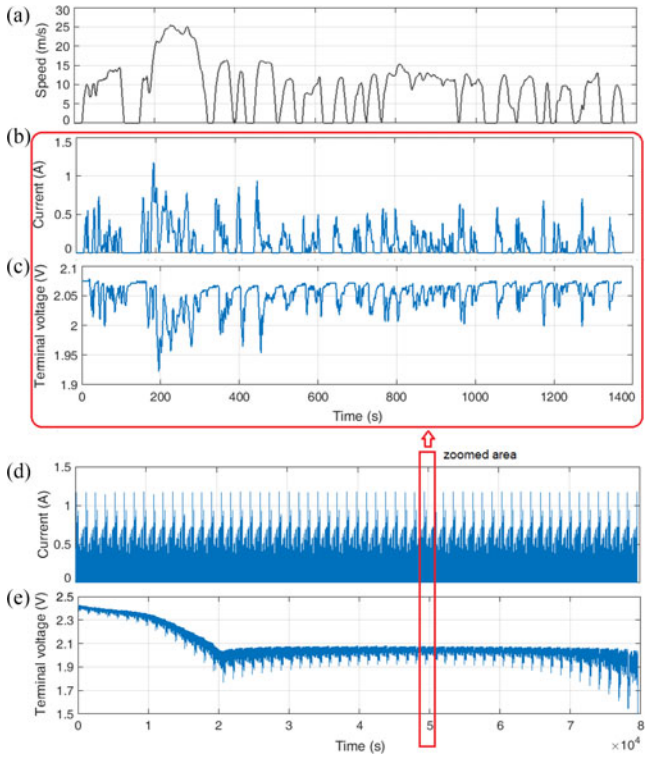

Fig. 14. Li-S cell discharge test based on UDDS drive cycle. (a) UDDS speed profile. (b) Li-S cell current profile based on one UDDS cycle. (c) Terminal voltage of a Li-S cell during one UDDS cycle. (d) Repeating UDDS current profile. (e) Li-S cell's terminal voltage during UDDS test.

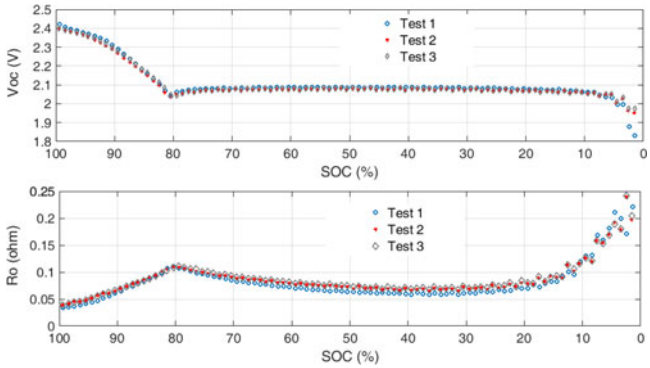

Fig. 15. Li-S cell parametrization at 30 °C during UDDS tests.

TABLE IV
Li-S Cell SOC Estimation Results of UDDS Tests

	Test 1	Test 2	Test 3
Temperature	30 °C	30 °C	30 °C
Maximum current	1.17 A	1.75 A	1.75 A
Average SOC estimation error	7.1%	6.2%	6.0%
Maximum SOC estimation error	20.9%	18.3%	21.1%

It is obvious in Fig. 15 that the identification accuracy decreases a bit at low SOC due to the fluctuations in ohmic resistance. We have called this "identification uncertainty area," depicted in Fig. 19. The Li-S cell's SOC estimation error in this area is mainly due to the identification error.

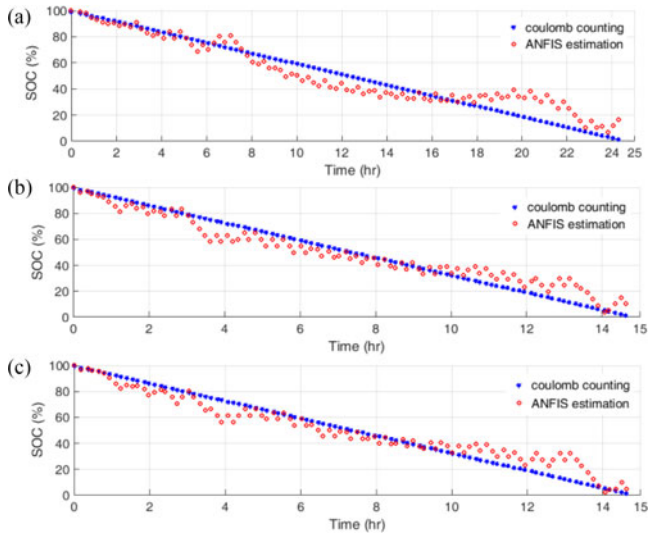

Fig. 16. Li-S cell SOC calculation using coulomb-counting and ANFIS estimation at 30 °C during UDDS tests. (a) Test 1. (b) Test 2. (c) Test 3.

Fig. 16 demonstrates SOC estimation results during the UDDS tests in Table IV. Coulomb counting is used here as a benchmark for validation of the estimation results. It is assumed that the total capacity, needed for coulomb counting, is available; however, it is not in a real application. Ideally, the total capacity is calculated after finishing each test. This is a good theoretical method to evaluate the estimation results. On the other hand, ANFIS SOC estimator can be used in a real application because it does not need to know cell's total capacity in advance. Li-S cell SOC estimation results of UDDS tests are presented in Table IV. The average and maximum error values are a bit higher in comparison to the previous results presented in Table III. This is due to more simplicity of the pulse discharge data comparing to a real discharge profile for EV application. Although the SOC estimation results are not perfect, they are not bad as outcome of a first study in this area. Generally, Li-S battery has much more complexities comparing to Li-ion and this study is just focused on one aspect that is SOC observability and estimation. Three main sources of error in Li-S cell's SOC estimation are as follows.

1) Shift in the breakpoint between high-plateau and low-plateau around 75% SOC: this can happen due to temperature change, high discharge rate, ageing, etc., and leads to an error in SOC estimation between 65% and 85% SOC.
2) Flat shape of OCV curve: this can cause a challenge in Li-S cell SOC estimation in the range of 15% to 75% SOC due to poor observability of the system as discussed here.
3) Identification uncertainty: generally, an error in cell model identification leads to an error in SOC estimation as well. However, this effect is dominant at low SOC range since the identification accuracy is less between zero and 30% SOC.

VII. Hybrid Technique for Li-S Cell SOC Estimation

Performance of the ANFIS SOC estimator was investigated in a real driving scenario in the previous section. The results demonstrate that ANFIS estimation error can increase to 20% in few points, which need to be improved. A solution which is proposed in this section is a hybrid estimation technique, which utilizes benefits of ANFIS and coulomb-counting methods at the same time. Referring back to the disadvantages of the coulomb-counting as discussed in the introduction section, this method is not applicable in practice because it can only start to estimate from a given initial SOC value, which is not always available in real conditions. In addition, coulomb-counting suffers from accumulated errors caused by noise and measurement errors [9], [10]. Another problem is that the battery capacity ($\mathrm{C_t}$) might change under various conditions, which can lead to errors when using coulomb-counting. On the other side, an ANFIS estimator has been developed in this study, it suffers from fluctuations that can lead to losing accuracy in a short time interval while the average accuracy is acceptable. In order to have the benefits of both techniques, a new hybrid estimation technique is proposed here, which is accurate and also applicable in real conditions. This hybrid technique consists of both the ANFIS and the coulomb-counting methods. A combination of these two would be able to determine the initial SOC value itself and compensate the effect of measurement noise and also it would have less fluctuations due to use of coulomb-counting as a limiting bound for ANFIS.

Mathematically, the hybrid estimation technique is formulated as follows:

$$\mathrm{SOC}_H = \frac{W_1 . \mathrm{SOC}_{\mathrm{ANFIS}} + W_2 . \mathrm{SOC}_{\mathrm{coulomb-counting}}}{W_1 + W_2} \tag{32}$$

$$WR = \frac{W_2}{W_1} \tag{33}$$

where SOC_H is the value of SOC provided by the hybrid technique, $\mathrm{SOC}_{\mathrm{ANFIS}}$ is the ANFIS estimation and $\mathrm{SOC}_{\mathrm{coulomb-counting}}$ is the value of SOC based on coulomb-counting. It should be noted that the coulomb-counting is restarted at each step by initializing from the previous estimation value (SOC_H). Consequently, there is no accumulated error in this technique. Two weight factors, W_1 and W_2, are considered to do a proper tradeoff between the two techniques. The weight ratio (WR) determines the role of each technique in this formulation. For example, a WR of 2 means that we trust two times more on coulomb-counting estimation in comparison to ANFIS estimation. This ratio can change over the whole range of SOC depending on the uncertainties of both techniques. For example, at the beginning, WR is considered to be zero ($W_1 = 1$ and $W_2 = 0$) since coulomb-counting is not able to determine the initial SOC. Particularly for Li-S cell, ANFIS estimation is more reliable at high-plateau (SOC more than 80%) so the weight of ANFIS is more in this area. On the other side, coulomb-counting can help more after passing a number of iterations, especially in the middle range of SOC.

In Fig. 17, Li-S cell SOC calculation using coulomb counting and the hybrid technique are illustrated over UDDS test at 30 °C. The test started from 80% SOC, but the initial value was not provided to any of the algorithms. Since the estimation algorithms do not know about the initial condition, both are started from 50% SOC. As demonstrated in the figure, the hybrid technique is able to converge to a close bound around the right value of SOC by using ANFIS capabilities. On the other hand,

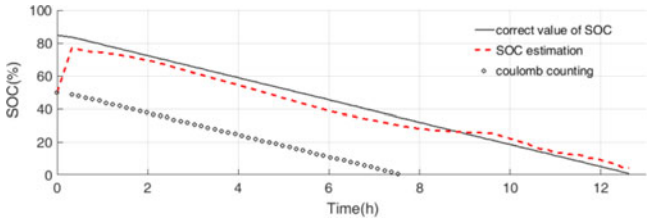

Fig. 17. SOC calculation using coulomb-counting and the hybrid technique over UDDS test at 30 °C, starting from 80% SOC.

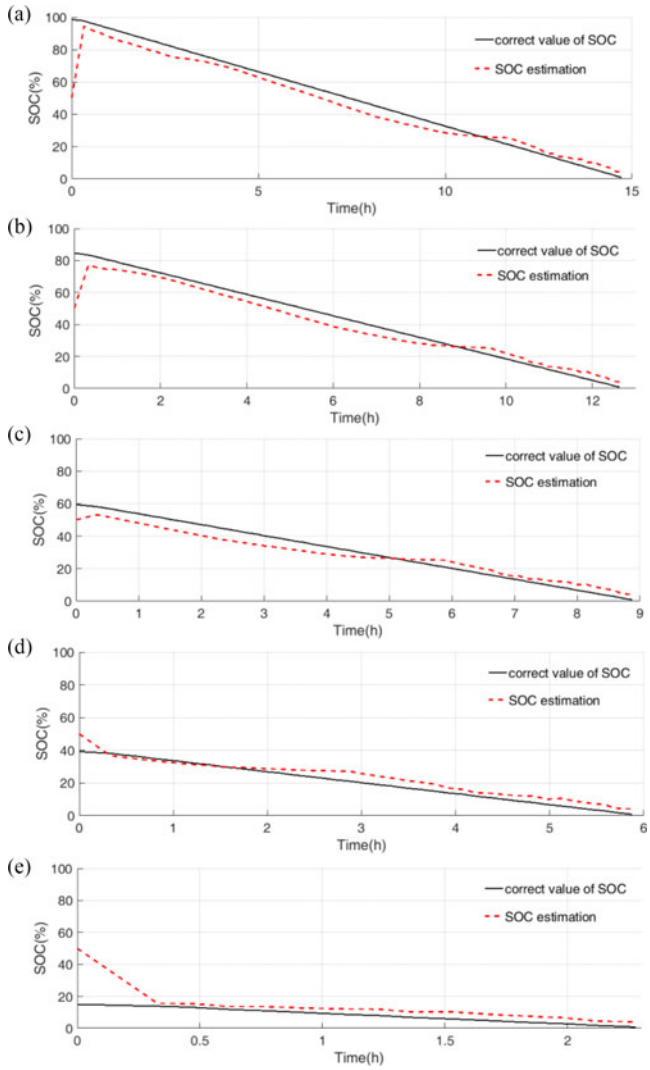

Fig. 18. Li-S cell SOC estimation over UDDS test at 30 °C using the hybrid technique from different initial conditions. (a) 100%. (b) 85%. (c) 60%. (d) 40%. (e) 15%.

coulomb-counting continues from 50%, which is not acceptable. Comparing the hybrid technique to ANFIS performance (presented in Fig. 16), it is obvious that the fluctuations are decreased a lot and consequently, the maximum error is controlled successfully by using coulomb-counting in combination of ANFIS. The proposed hybrid technique is tested at various initial conditions and the estimation results are presented in Fig. 18 and Table V. The results demonstrate that the proposed technique is able to converge to the right value of SOC from any initial condition and is able to keep going in a limited bound around it. Using this technique, a Li-S cell's SOC can be estimated with a mean error of 4%, and a worst-case error of 7% in a realistic driving scenario.

TABLE V
LI-S CELL SOC ESTIMATION ACCURACY USING THE HYBRID TECHNIQUE OVER UDDS TEST AT 30 °C WITH VARIOUS INITIAL SOC

Initial SOC (%)	Average SOC estimation error	Maximum SOC estimation error
100	4.18	6.64
85	4.03	6.66
60	4.13	6.93
40	2.91	6.01
15	3.08	4.51

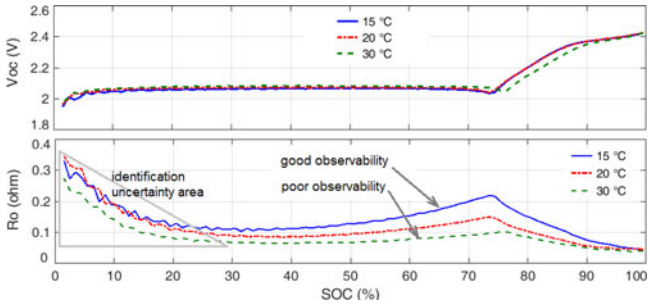

Fig. 19. Li-S cell parametrization at 15 °C, 20 °C, and 30 °C.

VIII. EFFECT OF TEMPERATURE

To investigate the effect of temperature, similar tests are repeated at different temperature levels. A thermal chamber is used to control the battery temperature during each test. Three temperature values, 15 °C, 20 °C, and 30 °C, are investigated in this study. Fig. 19 demonstrates the effect of temperature on Li-S cell model parametrization. As shown in this figure, temperature has a significant effect on Li-S cell's ohmic resistance. Temperature not only affects the resistance value, but also it changes the gradient of ohmic resistance with respect to SOC. So it can significantly affect the SOC estimation results by changing two inputs of the SOC estimator. Another interesting outcome of this plot is relevant to the observability analysis: the results demonstrate that Li-S cell's SOC observability becomes weaker at higher temperature values. The reason is the lower rate of change in ohmic resistance at higher temperature as depicted in Fig. 19. This means more challenge in Li-S cell SOC estimation at high temperature levels. It should be noted that the performance of the proposed framework was presented in Fig. 16 for our worst case that is at 30 °C.

On the other hand, Li-S cell's OCV curve is less affected by temperature; however, this result depends on SOC area as well. At high-plateau (from 100% SOC to the breakpoint around 75% SOC), OCV changes a bit in response to temperature variations. Indeed, the breakpoint happens earlier at a higher temperature due to the temperature-dependency of speed of the electrochemical reactions taking place inside the cell. At low-plateau (from

the breakpoint around 75% SOC to zero SOC), OCV curve is more stable, not much affected by temperature variation.

In our practical application, the BMS regulates the battery pack's temperature to ± 5 °C around a set point of 25 °C. When the temperature varies significantly, it is possible to use a set of estimators trained at different temperature levels. For example, assuming a set point of 25 °C, three separate estimators could be trained at 20 °C, 25 °C, and 30 °C. In this study, the effectiveness of our proposed technique was demonstrated in one case (i.e., 30 °C); however, this would be enough to conclude that same procedure can be repeated for other temperature values as well. The reason is that 30 °C is the worst case among them based on the observability results presented in Fig. 19. Although the effect of temperature on Li-S cell performance is discussed here briefly, we believe that more study is needed in this area.

IX. Conclusion

In this study, a new promising battery technology, i.e., Li-S, was investigated for application in automotive energy storage system. As a critical part of a Li-S BMS, an SOC estimation algorithm was proposed for a Li-S cell in this study for the first time. An observability analysis demonstrated that the Li-S cell's ECN model is not observable unlike Li-ion or NiMH battery types. This result, which is due to the flat shape of OCV-SOC curve of a Li-S cell, makes it more challenging than other battery technologies to be estimated and controlled.

Since the existing solutions in the literature were not suitable for this application, a new framework for online Li-S battery measurement, parameterization, and SOC estimation was designed and tested. It was demonstrated that using the proposed technique, a Li-S cell's SOC can be estimated with a mean error of 4% and a worst-case error of 7% in a realistic driving scenario. Although this result seems satisfactory as a first attempt in this area, the potential for improvement should be explored in future works: for example, more inputs and MFs could be used in the ANFIS structure; considering more parameters in the model and different number and types of MFs could improve the estimation results (at a cost of greater complexity). For the final application of the study in an automotive energy storage system, the tradeoff between accuracy and speed (i.e., low-complexity) should be explored to find the best compromise.

One of the drawbacks of black-box intelligent approaches like ANFIS is that they need a large quantity of training data, which is sometimes not easy to obtain. Correct SOC estimation under a certain condition depends on consideration of a very similar condition in the training data. In the automotive application considered, variation of temperature and battery ageing could affect the estimator's performance significantly; in the initial study described in this paper, temperature and SOH effects were not investigated and more experiments would be needed for training ANFIS under a wide range of conditions.

Acknowledgment

This work was undertaken as part of two projects: the "Revolutionary Electric Vehicle Battery" project, supported by the Innovate UK/EPSRC under Grant TS/L000903/1 and Grant EP/L505286/1, and the "Understanding Future Vehicles" project supported by the EPSRC under Grant EP/I038586/1. Data underlying this study can be accessed through the Cranfield University repository at http://dx.doi.org/10.17862/cranfield.rd.5297209.

References

[1] A. F. Hofmann, D. N. Fronczek, and W. G. Bessler, "Mechanistic modeling of polysulfide shuttle and capacity loss in lithium-sulfur batteries," *J. Power Sources*, vol. 259, pp. 300–310, 2014.

[2] L. Lam and P. Bauer, "Practical capacity fading model for li-ion battery cells in electric vehicles," *IEEE Trans. Power Electron.*, vol. 28, no. 2, pp. 5910–5918, Dec. 2013.

[3] I. S. Kim, "Nonlinear state of charge estimator for hybrid electric vehicle battery," *IEEE Trans. Power Electron.*, vol. 23, no. 4, pp. 2027–2034, Jul. 2008.

[4] J. C. A. Anto´n, P. J. G. Nieto, F. J. de Cos Juez, F. S. Lasheras, C. B. Viejo, and N. R. Guti´errez, "Battery state-of-charge estimator using the MARS technique," *IEEE Trans. Power Electron.*, vol. 28, no. 8, pp. 3798–3805, Aug. 2013.

[5] J. C. A. Anto´n, P. J. G. Nieto, C. B. Viejo, and J. A. V. Vil´an, "Support vector machines used to estimate the battery state of charge," *IEEE Trans. Power Electron.*, vol. 28, no. 12, pp. 5919–5926, Dec. 2013.

[6] M. Ugras Cuma and T. Koroglu, "A comprehensive review on estimation strategies used in hybrid and battery electric vehicles," *Renew. Sustain. Energy Rev.*, vol. 42, pp. 517–531, 2015.

[7] J. Li, J. K. Barillas, C. Guenther, and M. A. Danzer, "A comparative study of state of charge estimation algorithms for LiFePO4 batteries used in electric vehicles" *J. Power Sources*, vol. 230, pp. 244–250, 2013.

[8] C. H. Cai, D. Du, and Z. Y. Liu, "Battery state-of-charge (SOC) estimation using adaptive neuro-fuzzy inference system (ANFIS)," in *Proc. 12th Int. Conf. IEEE Fuzzy Syst.*, 2003, vol. 2, pp. 1068–1073.

[9] B. Pattipati, C. Sankavaram, and K. Pattipati, "System identification and estimation framework for pivotal automotive battery management system characteristics," *IEEE Trans. Syst., Man, Cybern. C, Appl. Rev.*, vol. 41, no. 6, pp. 869–884, Nov. 2011.

[10] K. Kutluay, Y. Cadirci, Y. S. Ozkazanc, and I. Cadirci, "A new online state-of-charge estimation and monitoring system for sealed lead-acid batteries in telecommunication power supplies," *IEEE Trans. Ind. Electron.*, vol. 52, no. 5, pp. 1315–1327, Oct. 2005.

[11] L. Zhong, C. Zhang, Y. He, and Z. Chen, "A method for the estimation of the battery pack state of charge based on in-pack cells uniformity analysis," *Appl. Energy*, vol. 113, pp. 558–564, 2014.

[12] X. Liu, Z. Chen, C. Zhang, and J. Wu, "A novel temperature-compensated model for power Li-ion batteries with dual-particle-filter state of charge estimation," *Appl. Energy*, vol. 123, pp. 263–272, 2014.

[13] S. Schwunk, N. Armbruster, S. Straub, J. Kehl, and M. Vetter, "Particle filter for state of charge and state of health estimation for lithium–iron phosphate batteries," *J. Power Sources*, vol. 239, pp. 705–710, 2013.

[14] C. Zheng, Y. Fu, and C. C. Mi, "State of charge estimation of lithium-ion batteries in electric drive vehicles using extended Kalman filtering," *IEEE Trans. Veh. Technol.*, vol. 62, no. 3, pp. 1020–1030, Mar. 2013.

[15] H. Rahimi-Eichi, F. Baronti, and M. Y. Chow, "Online adaptive parameter identification and state-of-charge coestimation for lithium-polymer battery cells," *IEEE Trans. Ind. Electron.*, vol. 61, no. 4, pp. 2053–2061, Apr. 2014.

[16] W. He, N. Williard, C. Chen, and M. Pecht, "State of charge estimation for electric vehicle batteries using unscented Kalman filtering," *Microelectron. Rel.*, vol. 53, no. 6, pp. 840–847, 2013.

[17] G. L. Plett, "Extended Kalman filtering for battery management systems of LiPB-based HEV battery packs: Part 1. Background," *J. Power Sources*, vol. 134, pp. 252–261, 2004.

[18] G. L. Plett, "Sigma-point Kalman filtering for battery management systems of LiPB-based HEV battery packs, Part 2: Simultaneous state and parameter estimation," *J. Power Sources*, vol. 161, pp. 1369–1384, 2006.

[19] F. Sun, X. Hu, Y. Zou, and S. Li, "Adaptive unscented Kalman filtering for state of charge estimation of a lithium-ion battery for electric vehicles," *Energy*, vol. 36, no. 5, pp. 3531–3540, 2011.

[20] H. He, R. Xiong, X. Zhang, F. Sun, and J. X. Fan, "State-of-charge estimation of the lithium-ion battery using an adaptive extended Kalman filter based on an improved Thevenin model," *IEEE Trans. Veh. Technol.*, vol. 60, no. 4, pp. 1461–1469, May 2011.

[21] Y. Tian, B. Xia, W. Sun, Z. Xu, and W. Zheng, "A modified model based state of charge estimation of power lithium-ion batteries using unscented Kalman filter," *J. Power Sources*, vol. 270, pp. 619–626, 2014.
[22] J. Xu, C. C. Mi, B. Cao, J. Deng, Z. Chen, and S. Li, "The state of charge estimation of lithium-ion batteries based on a proportional-integral observer," *IEEE Trans. Veh. Technol.*, vol. 63, no. 4, pp. 1614–1621, May 2014.
[23] L. Ljung, *System Identification—Theory For the User*. New York, NY, USA: Prentice-Hall, 1987.
[24] C. H. Cai, D. Du, and Z. Y. Liu, "Battery state-of-charge (SOC) estimation using adaptive neuro-fuzzy inference system (ANFIS)," in *Proc. Int. Conf. IEEE Fuzzy Syst.*, 2003, vol. 2, pp. 1068–1073.
[25] M. F. Tsai, Y. Y. Peng, C. S. Tseng, and N. S. Li, "Modeling and estimation of state of charge for lithium-ion batteries using ANFIS architecture," in *Proc. Int. Symp. IEEE Ind. Electron.*, Hangzhou, China, 2012, pp. 863–868.
[26] [Online]. Available: http://www.oxisenergy.com
[27] A. Fotouhi, D. J. Auger, K. Propp, S. Longo, and M. Wild, "A review on electric vehicle battery modelling: From lithium-ion toward lithium-sulphur," *Renew. Sustain. Energy Rev.*, vol. 56, 1008–1021, 2016.
[28] M. Thele, O. Bohlen, D. U. Sauer, and E. Karden, "Development of a voltage-behavior model for NiMH batteries using an impedance-based modeling concept," *J. Power Sources*, vol. 175, pp. 635–643, 2008.
[29] H. He, R. Xiong, and J. Fan, "Evaluation of lithium-ion battery equivalent circuit models for state of charge estimation by an experimental approach," *Energies*, vol. 4, pp. 582–598, 2011.
[30] V. H. Johnson, "Battery performance models in ADVISOR," *J. Power Sources*, vol. 110, pp. 321–329, 2002.
[31] D. J. Leith and W. E. Leithead, "Survey of gain-scheduling analysis and design," *Int. J. Control*, vol. 73, no. 11, pp. 1001–1025, 2000.
[32] K. Ogata, *Modern Control Engineering*, 5th ed. Englewood Cliffs, NJ, USA: Prentice-Hall, 2010.
[33] Z. M. Salameh, M. A. Casacca, and W. A. Lynch, "A mathematical model for lead-acid batteries," *IEEE Trans. Energy Convers.*, vol. 7, no. 1, pp. 93–98, Mar. 1992.
[34] A. Fotouhi, K. Propp, and D. J. Auger, "Electric vehicle battery model identification and state of charge estimation in real world driving cycles," in *Proc. 7th Int. Conf. Comput. Sci. Electron. Eng.*, Colchester, U.K., 2015, pp. 243–248.
[35] A. Fotouhi, D. J. Auger, K. Propp, and S. Longo, "Electric vehicle battery parameter identification and SOC observability analysis: NiMH and Li-S case studies," *IET Power Elect.*, vol. 10, no. 11, 2017, pp. 1289–1297.
[36] I. S. Kim, "A technique for estimating the state of health of lithium batteries through a dual-sliding-mode observer," *IEEE Trans. Power Electron.*, vol. 25, no. 4, pp. 1013–1022, Apr. 2010.
[37] [Online]. Available: https://www.dieselnet.com/standards/cycles/ftp72.php
[38] A. Fotouhi *et al.*, "A MATLAB graphical user interface for battery design and simulation; From cell test data to real-world automotive simulation." in *Proc. 13th Int. Conf. Synthesis Model. Anal. Simul. Methods Appl. Circuit Design*, Lisbon, Portugal, 2016, doi: 10.1109/SMACD.2016.7520715

Abbas Fotouhi (M'13) received the Ph.D. degree in mechanical engineering from Iran University of Science and Technology, Tehran, Iran, in 2011.

He started his academic career as a Lecturer in Islamic Azad University, Iran. He, then, joined the Centre for Artificial Intelligence and Robotics, University Technology Malaysia. Since 2014, he has been with the Advanced Vehicle Engineering Centre, Cranfield University, Cranfield, U.K. His specialty is modeling and simulation, identification, control and optimization, artificial intelligence, and machine learning. His current research interests include battery technology, vehicle powertrain design and optimization, and intelligent mobility. He is associate editor of the International Journal of Strategic Engineering, editorial board member of Neural Computing and Applications Journal, and member of the IEEE and the Electrochemical Society.

Daniel J. Auger (SM'15) received the M.Eng. and Ph.D. degrees in control engineering, specializing in model validation for robust feedback control design, from the University of Cambridge, Cambridge, U. K., in 2000 and 2005, respectively.

He is currently a Lecturer in advanced control and optimization in Cranfield University, Cranfield, U.K. His current research interests include the application of advanced control methodologies to automotive design, development of software-embeddable battery models, optimal state-estimator design, and robust control architectures. His recent publications have looked at multiobjective optimization of electrified powertrains, embeddable models of lithium-sulfur batteries, and advanced techniques for battery state estimation.

Karsten Propp received the Master of Automotive Engineering degree from the University of Applied Sciences, Berlin, Germany, in 2013 and the Ph.D. degree under supervision of Dr. Daniel J. Auger in Advanced Vehicle Engineering Centre, Cranfield University, Cranfield, U. K, in 2017.

His research interest includes development of advanced control algorithms for vehicle battery management systems applicable for lithium sulfur cells.

Stefano Longo (SM'16) received the M.Sc. degree in control systems from the University of Sheffield, Sheffield, U.K., in 2007, and the Ph.D. degree in networked control systems from the University of Bristol, Bristol, U.K., in 2011.

Since 2012, he has been a Lecturer (Assistant Professor) of vehicle electronics and control in Cranfield University, Cranfield, U.K. His Ph.D. thesis received the Institution of Engineering and Technology (IET) Control and Automation Prize for significant achievements in the area of control engineering. In November 2010, he was appointed to the position of Research Associate in Imperial College London, London, U.K.

Dr. Longo is currently the Course Director for the M.Sc. degree in automotive mechatronics, Associate Editor of the *Elsevier Journal on Mechatronics*, elected executive member of the *IET Control and Automation Network*, and member of the IFAC technical committee on Mechatronic Systems.